Structure–property relationship study of the HPLC enantioselective retention of neuroprotective 7-[(1-alkylpiperidin-3-yl)methoxy]coumarin derivatives on an amylose-based chiral stationary phase

Leonardo Pisani, Mariagrazia Rullo, Marco Catto, Modesto de Candia, Antonio Carrieri, Saverio Cellamare, Cosimo D. Altomare*

Department of Pharmacy-Drug Sciences, University of Bari Aldo Moro, Bari, Italy

Running title: HPLC resolution of coumarin derivatives on amylose-based chiral stationary phase

Correspondence: Prof. Cosimo Damiano Altomare, Department of Pharmacy-Drug Sciences, University of Bari Aldo Moro, Via E. Orabona 4, 70125 Bari, Italy

E-mail: cosimodamiano.altomare@uniba.it

Fax: +39-080-5442230

Abbreviations: **ADMPC**, amylose tris(3,5-dimethylphenylcarbamate); **CS**, chiral selector; **CSP**, chiral stationary phase; **LFER**, linear free energy relationship; **HB**, hydrogen bond; **MeOH**, methanol; **NP**, normal-phase; **QSPR**, quantitative structure–property relationship; **SA**, selectand.

Keywords: coumarins / Chiral recognition / Linear free energy relationships / Molecular docking / Polysaccharides /

Abstract

The enantiomer separation of a number of racemic 7-[(1-alkylpiperidin-3-yl)methoxy]coumarin derivatives, some of which show outstanding in vitro multitarget neuroprotective activities, was successfully achieved on a polysaccharide-based chiral

Received: 12 06, 2017; Revised: 01 29, 2018; Accepted: 01 29, 2018

This article has been accepted for publication and undergone full peer review but has not been through the copyediting, typesetting, pagination and proofreading process, which may lead to differences between this version and the Version of Record. Please cite this article as doi: 10.1002/jssc.201701442 .

stationary phase, bearing amylose tris(3,5-dimethylphenylcarbamate) as chiral selector, in normal polar mode (methanol and acetonitrile as the mobile phases). The majority of the screened selectands, especially those bearing 1-(3-X-benzyl)piperidin-3-yl moieties, showed baseline enantiomer separations, and compound **8** (X = NO_2) was the best resolved (α = 2.01; R_S = 4.27). Linear free-energy relationships, usefully complemented by molecular docking calculations, proved the key role in enantioselective retention of aromatic interactions between π-donor moieties in the chiral selector and π-acceptor moieties in selectand, strengthened by hydrogen bond interaction between a hydrogen bond donor in the chiral selector and the hydrogen bond acceptor group(s) in the selectand. Statistically reliable equations highlighted the importance of the substituent's size and substitution pattern (*meta* better than *para*) to affect the enantiorecognition of the title compounds. The chromatographic data support the scalability of the optimized experimental conditions for preparative purposes.

1 Introduction

Direct LC with chiral stationary phases (CSPs) has long been established as a major tool in drug discovery, due to its reliability and versatility either for analytical (e.g. QC, pharmacokinetic profiling of enantiomeric drugs) and preparative purposes (i.e. access to individual enantiomers for pharmacological testing) [1-3]. Hundreds of CSPs have been developed over the last three decades, but a major advance in chiral chromatography was the introduction in the 1980s of the polysaccharide-based (cellulose or amylose backbone) CSPs [4], which allow several types of organic solvents to be used as the mobile phases and a wide range of racemates to be successfully resolved [5, 6].

The great enantiomer recognition potential of polysaccharide-based CSP stems from a number of structural properties, hierarchically ordered as follows: (i) molecular chirality due to the presence of several stereogenic centers of the glucose units, (ii) chiral folding due to helical twist of the polymer backbone, and (iii) supramolecular chirality resulting from the alignment of the adjacent polymer chains which form ordered regions, as proven by X-ray diffraction [7]. An important factor affecting the enantiomer recognition potential of these CSPs is the functionalization pattern of the glucose OHs usually with substituted phenyl carbamates or esters, which contribute to form a regular arrangement of grooves and suitable enantioselective binding pockets along the polysaccharide chain. Based on NMR and computational studies, Yamamoto et al. suggested a highly organized left-handed 4/3 helical structure for amylose tris(3,5-dimethylphenylcarbamate) (ADMPC), in which the aromatic moieties may be involved in face-to-face or face-to-edge π–π interactions [8]. The carbamate functionalities should allow conformational adjustment (induced fit) of the aromatic moieties, as to maximize their π–π interactions, thereby stabilizing the transient diastereomeric complex between chiral selector (CS) and selectand (SA) through hydrogen bond (HB) and polar interactions [9].

Within a long-standing research program aimed at developing new multitarget small molecules for the treatment of neurological multifactorial disorders, including Alzheimer's disease (AD) [10-13], we recently reported a wide series of 1-benzyl-piperidin-3-yl and piperidin-4-yl derivatives of 7-hydroxy-3,4-dimethyl-coumarin [14]. These compounds are potent inhibitors of monoamine oxidase B (MAO B) and acetylcholinesterase (AChE) with good selectivity over the two respective isoforms (MAO A and butyrylcholinesterase, BChE). The chiral piperidin-3-yl derivatives are more water-soluble and less lipophilic than their piperidin-4-yl isomers. They showed higher potencies in human MAO B inhibition, achieving two-digit nanomolar values of IC_{50}s, while maintaining AChE inhibition potency in

the low micromolar range. Semi-preparative resolution of racemic compounds **3** and **4** were successfully accomplished, by using an amylose-based CSP (Chiralpak IA column, Fig. 1B) which bears ADMPC as chiral selector (CS). The eutomer (+)-**3** showed an outstanding *h*MAO B affinity (IC_{50} = 23 nM), with eudismic ratio of 8.5, about 170-fold selectivity over MAO A and a good inhibition potency against AChE (IC_{50} = 1.80 μM). To extend our knowledge about the enantioselective binding toward MAO B and other targets involved in the multifactorial etiology of AD, we investigated the enantiomer resolution of a number of other *rac*-7-[(1-alkylpiperidin-3-yl)methoxy]coumarin derivatives by two amylose-based CSPs (Fig. 1).

In this study, we report on the optimization of the experimental conditions to achieve baseline separation of the racemic compounds **1–16**, by using the above-mentioned CSPs in normal polar mode (MeOH and ACN, or their combinations, as the mobile phases). An extrathermodynamic approach, complemented with molecular docking calculation, was applied to detect the main physicochemical determinants involved in chiral recognition of the 1-benzylpiperidin-3-yl-coumarin selectands by the investigated amylose-based CS.

2 Materials and methods

2.1 Chemicals

Starting materials, reagents, catalysts, analytical grade solvents and HPLC grade solvents were purchased from Sigma–Aldrich (Milan, Italy). Synthesis and analytical data of compounds **1**, **3–5**, **9**, **10**, **13**, **14** and **16** have been previously reported [14]. Compounds **2**, **6–8**, **11**, **12** and **15**, and related intermediates, were synthesized in this study, following similar procedures with slight modifications (Supporting Information).

2.2 Apparatus and chromatography

The analytical HPLC measurements were performed on a Waters 1525 HPLC System equipped with a Waters 2487 variable-wavelength UV-Vis detector, and a Waters 717 plus autosampler; the chromatographic data were acquired using the Waters Breeze Software (Waters, Sesto San Giovanni, MI, Italy). Lux® 5µ Amylose-2 and Chiralpak® IA columns, used as CSPs, were purchased from Phenomenex (Castel Maggiore, BO, Italy) and Daicel (Chiral Technologies Europe, Illkirch Cedex, France), respectively. Both columns were 5 µm, 150×4.6 mm, stainless-steel columns. The analytes were solubilized in MeOH at 1 mM concentration. The mobile phases were filtered through a PTFE membrane (0.45 µm) before use.

A preliminary screening was performed on both CSPs in polar mode by using MeOH and ACN, or their v/v combinations, as the mobile phases, to optimize the conditions for enantiomer resolution. Capacity factor (*k*'), enantioselectivity (α) and resolution (R_S) data are summarized in Table 1.

2.3 Determination of lipophilicity

Lipophilicity parameters of the racemic (**1–16**, Table 1) and achiral compounds **17–25** (Supporting Information, Table S3) were measured by an RP-HPLC technique [15, 16]. MeOH solutions of the investigated compounds (1 mM) were filtered through a Nylon-66 membrane 0.45 µm (Supelco, USA) and injected into HPLC equipped with Zorbax Eclipse-C18 column (5 µm, 250×4.6 mm), from Agilent Technologies (Cernusco sul Naviglio, MI, Italy). Each compound was eluted at different mobile phase composition (ranging from 0.9 to 0.5% MeOH in 20 mM ammonium acetate buffer at pH 4.00; 0.05% MeOH increments). All RP-HPLC measurements were carried out at 25 ± 1°C, flow rate of 1.0 mL/min and 320 nm wavelength on Agilent 1260 Infinity Quaternary Pump equipped with Agilent 1260 Infinity

Diode Array Detector and Agilent 1260 Infinity Standard Autosampler (Agilent Technologies, Cernusco sul Naviglio, MI, Italy).

The logarithm of capacity factor ($\log k' = \log (t_R - t_0)/t_0$) of each compound at different mobile phase compositions has been calculated; t_R represents the retention time of the solute and t_0 is the column dead time, measured as the retention time of a KI solution in MeOH. For each compound, the $\log k'$ value increased linearly with decreasing MeOH volume fraction. The logarithm of capacity factor extrapolated to 100% aqueous mobile phase ($\log k'_w$) was calculated from the linear regressions on at least five data points.

Lipophilicity was also computationally assessed with ACDLabs software, release 9.0 (Advanced Chemistry Development, Toronto, Canada).

2.5 Molecular Modeling

Molecular models of the chiral selectands (**1–16**) were built in both neutral and protonated forms, using standard bond lengths and valence angles, with Maestro [17], and charges were calculated according to the Gasteiger method using the molcharge suite of QUACPAC [18]. The 3D skeleton of the chiral selector of Chiralpak IA stationary phase was assembled starting from the two left-handed double helix of α-amylose deposited in the PolySac3Db [19], replicating the structural data achieved by Imberty et al. [20]. Twelve units of chain A were selected, and 3,5-dimethylphenyl-carbamoyl moieties were linked to all the hydroxyl groups of each α-glucose monomer, further relaxing the whole structure with the Maestro software package. To achieve a plausible low energy conformation representation, the ADMPC (12-mer) model was then subjected to a short molecular dynamics (MD) simulation. Using the Desmond system builder tool implemented in Maestro [21], a solvated model was assembled merging the oligoamylose molecular entity (12-mer ADMPC) in a 69908 $Å^3$ orthorhombic box filled with MeOH molecules mimicking the mobile phase. All simulations

were performed on a NVDIA Quadro M4000 GPU at constant temperature (300 K) and pressure (1 bar) for a total of 180 ns using the default settings and relaxation protocol of Desmond [22], with energy and trajectory recording interval of 60 ps. From the achieved trajectories, the frame endowing the lowest potential energy was selected for the docking study.

The docking study was carried out with AutoDock 4.2 [23], loading Gasteiger charges to the oligosaccharide units and calculating the affinity maps on a 125×100×150 Å (0.375 Å spaced) rectangular box centered on the target structure. In a first instance, the model of the best enantioresolved compound **8**, in *S* and *R* configurations, was subjected to a total of 500 Lamarckian Genetic Algorithm (LGA) runs, setting the population size and the number of energy evaluations to 150 and 5 million, respectively, and randomizing at each run the value of the initial coordinates for the center of the ligand (tran0), ligand rigid-body orientation (quat0) and relative dihedral angles (dihe0). All poses were then clustered to RMSD of 2.0, and ranked according to the relative Free Energy of Binding (FEB) [24]. The best FEB pose of *rac*-**8** was thereafter selected as template for determining through a superposition achieved by means of the ROCS vers. 3.2.1.4 (OpenEye Scientific Software, Santa Fe, NM, US), a shape- and atom-based matching algorithm, the initial pose of the other racemic compounds, and thereafter with AutoDock the final binding mode of the rest of selectands [25]. To address this topic for each selectand of the examined data set the maximum number conformers was generated with OMEGA ver. 2.5.1.4 (OpenEye Scientific Software, Santa Fe, NM, US) [26], and the ROCS shape objective function was used for ranking the ligand database, and for selecting the best molecular alignment, according to the Tanimoto coefficient. Starting from this overlay, 1000 independent runs were performed for each compound, and the best and most populated FEB pose was identified using Autodock with the same docking parameters of compound **8**. Due to complexity of the target surface, which

might shows multiple binding site, and to validate our protocol, the same docking procedure of compound **8** was then repeated for compound **2**, and a comparable binding mode was achieved. The Autodock setting file is reported in Supporting Information.

3 Results and discussion

A number of already reported [14] and newly synthesized racemic compounds (*rac*-**1–16**) were screened on two amylose-based CSPs (Fig. 1) used in normal polar mode (MeOH and ACN, or their combination, as the mobile phases) to optimize the experimental conditions for a good performance in terms of enantioselectivity (α) and resolution (R_S). A number of achiral 1-piperidin-4-yl derivatives (**17–25**, Supporting Information) were also screened, to highlight the physicochemical properties mainly modulating retention on the amylose-based CSP.

The investigated CSPs differ not only for CS (Fig. 1), but also for their silica matrix stabilities. Lux Amylose-2 column (Fig. 1A) is packed with the derivatized amylose coated on silica, compatible with normal phase, RP or polar organic modes, but requires to avoid the use of solvents other than water, alcohols, acetonitrile and mixtures thereof. In contrast, Chiralpak IA column (Fig. 1B) is packed with an amylose-based selector (ADMPC) immobilized on a wide pore silica matrix, which confers to the CSP a wider solvent compatibility.

Separation of the *N*-benzyl racemic compounds **3**, **4** and **8** was evaluated on Lux Amylose-2 by changing both mobile phase composition (MeOH and ACN) and flow rate (0.5 and 1.0 mL/min). With 100% ACN mobile phase, only *rac*-**4** (R = 3-bromophenyl) and *rac*-**8** (R = 3-nitrophenyl) showed enantiomer selectivity, but with no baseline separation (Fig. S3, Supporting Information). In contrast, with Chiralpak IA and MeOH eluent at 1.0 mL/min

flow rate, a good baseline separation of *rac*-**3** (R = phenyl) was successfully achieved (Fig. S2, Supporting Information).

The mobile phase composition allowing the baseline separation of the majority of the racemic compounds was MeOH/ACN, 8:2 v/v at 1 mL/min flow rate (Fig. 2). Among the investigated selectands, the 3-nitrobenzyl derivative showed the highest resolution ($\alpha = 2.01$; $R_S = 4.27$). The chromatographic data in Table 1 and in Tables S1 and S2 (Supporting Information) show that Chiralpak IA column performed better than Lux Amylose-2 in achieving enantiomer resolution of the *rac*-7-[(1-alkylpiperidin-3-yl)methoxy]coumarin derivatives.

A first look at the data in Table 1 suggests some trends of structure-property relationships. The *N*-$CH_2CH_2CH_2OH$ derivative (*rac*-**2**), compared to the *N*-CH_3 one (*rac*-**1**), achieved good enantiomer separation ($\alpha = 3.83$; $R_S = 1.97$), apparently due to enantiodiscrimination effect of the OH group, which may serve as HB acceptor in the interaction with the carbamoyl NH of the CS (Fig. S5, Supporting Information). The N-benzyl derivative *rac*-**3** showed good enantioselectivity and resolution ($\alpha = 1.83$; $R_S = 2.50$), likely due to π–π stacking interactions of the benzyl group, as supported by results of molecular docking calculations (Fig. S5).

Regarding the substituents on the benzyl group, F in *meta* (and not in *para*) position (*rac*-**6**) did not increase enantioselectivity compared to H (*rac*-**3**), whereas 3-Cl led to a decrease of α. A significant 'jump' in enantiomer separation and resolution was obtained with the 3-NO_2 (and not 4-NO_2) substituent. A slight increase of enantiomer separation over *rac*-**3** was observed for the CH_2OH substituent only in *meta* position (*rac*-**7**). From the enantioseparation data related to the *N*-benzyl derivatives (Table 1), it can be deduced that: (i) electron-withdrawing substituents do increase the enantioselectivity, in comparison with **3** (R = Ph), more than electron-donor substituents; (ii) with the same aromatic substituent (i.e. Cl, F, CH_2OH and NO_2), the *meta*-substituted derivatives show higher α values than the *para*-

substituted derivatives, most likely due to issues related to size and shape complementarity between SA and CS; (iii) with some exception (e.g., 4-OCH_3), enantioseparation decreases depending upon the size of the substituent (lack of steric fit), as shown for example by **12** and **13** (NO_2 and SO_2CH_3 differs significantly for their van der Waals volumes, which are 1.20 and 2.85, respectively).

To place the above trends on quantitative basis, we assessed lipophilicity of the investigated selectands. The piperidinyl-coumarin derivatives are bases with pK_a values ranging from 9.5–10 for the N-alkyl derivatives (**1** and **2**) to 8.3–8.9 for the *N*-benzyl derivatives (**3–16**). The pK_a value of the N-benzyl compound **3** was determined through ^{1}H NMR spectroscopy [27] and found to be 8.02 (Supporting Information). An average pK_a of 7.99 was determined for the corresponding achiral 1-benzylpiperidin-4-yl derivative (not shown). A pK_a shift toward lower values can be reasonably supposed in the solvents used in chiral HPLC [28].

Lipophilicity of all the racemic selectands **1–16** (and the achiral derivatives **17–25**; Supporting Information) was assessed through an RP-HPLC technique and by computational tools (ACDLabs software, release 9.0). A C18 column was used as the stationary phase, and capacity factors (*k*') of each compound were determined at different mobile phase composition as detailed in Materials and methods. For each compound, the log *k*' value increased linearly ($r^2 > 0.96$) with decreasing MeOH volume fraction; the linear relationships were extrapolated to 100% aqueous mobile phase to estimate log k'_w values. The examined compounds should be totally protonated at pH 4 (pK_a – pH > 2 log units), whereby log k'_w values should account for the lipophilicity of the ionized species. Distribution coefficients at pH 4.00 (CLOGD) were calculated by ACDLabs software and reported, along with log k'_w values, in Table 1 (**1–16**) and Table S3 (**17–25**). A graphical comparison between the capacity factors measured in enantioselective HPLC and log k'_w or CLOGD values did not

show any noteworthy relationship, in contrast with previous observations of ours with different series of SAs and CSPs [29-31].

An extrathermodynamic approach to the study of QSPRs was limited to the *N*-benzyl derivatives **2–16**. The properties of the substituents on the phenyl ring were described by the following parameters [32, 33]: (i) Hammett sigma constant (σ), which should account for the effect of the aromatic substituent on the electronic interactions with aromatic counterparts in the CS (face-to-face and face-to-edge π–π interactions, dipole–dipole interactions, etc.); (ii) molar refractivity (MR) and van der Waals volume (V_W), which may account for steric fitting of the phenyl substituents into the binding site of the CS; (iii) the Hansch lipophilic constant for the aromatic substituents (π_{ar}) and fragment lipophilic value calculated from log k'_w (τ). The parameters used as the independent variables in multiple linear regression (MLR) analysis, carried out according the ordinary least-squares (OLS) with leave-one-out (LOO) cross-validation (STATIST program [34]), are collected in Table S4 (Supporting Information), whereas the correlation matrix of the enantiomer separation data and parameters of the substituents of *rac*-**3–16** is shown in Table 2.

The capacity factor of the first eluted enantiomer (log k'_1) seems to be more sensitive to the electronic property of the substituent on the phenyl group, as described by the Hammett constant σ (Table 2). A scatter plot (Fig. S4, Supporting Information) showed a trend of linear relation which holds for electron-withdrawing groups. Indeed, for congeners bearing X groups with $\sigma \geq 0$ (omitting **3**, **7**, **15** and **16**), the following linear equation was obtained:

$$\log k'_1 = 0.58\ (\pm 0.08)\ \sigma + 0.07\ (\pm 0.04) \quad (1)$$

$n = 10$, $r^2 = 0.8631$, $q^2 = 0.8069$, $s = 0.0669$, $F = 50.44$

where n represents the number of data points, r^2 the coefficient of determination (squared correlation coefficient), q^2 the LOO cross-validation coefficient, s the SD of the regression equation, and F is the statistical significance of fit; 95% confidence intervals of the regression coefficients are given in parentheses.

Assuming σ as an indicator of the propensity to achieve π–π interactions (the higher sigma value, the higher π-acceptor feature of the phenyl ring in SA, the higher propensity to interact with the π-donor 3,5-dimethylphenyl moiety in CS) and polar interactions, retention of the piperidin-3-yl coumarin SAs on the amylose-based Chiralpak IA is mainly modulated by π–π interactions (eq. 1) involving the *meta*- and *para*-substituted phenyl group. The positive deviation from the linear eq. 1 of the methoxy congeners **15** and **16** may be reasonable, taking into account the capacity of the OCH_3 group(s) to form HBs with HB donor groups (e.g. the carbamoyl NH) in CS. The positive and negative deviations of **3** and **7** from eq. 1 are difficult to explain. No noteworthy linear equation was obtained for log k'_2, most likely because of the higher influence of steric fit in modulating the retention of the second-eluted enantiomers.

The regression analysis of the retention of achiral piperidin-4-yl derivatives (**18**–**25**, Supporting Information) with the same descriptors yielded the following equations:

$$\log k' = 1.91\ (\pm 0.35)\ \sigma - 0.18\ (\pm 0.13) \qquad (2)$$

$n = 8$, $r^2 = 0.8305$, $q^2 = 0.7323$, $s = 0.3294$, $F = 29.39$

$$\log k' = 2.20\ (\pm 0.34)\ \sigma - 0.58\ (\pm 0.32)\ V_W + 0.09\ (\pm 0.19) \qquad (3)$$

$n = 8$, $r^2 = 0.8971$, $q^2 = 0.6953$, $s = 0.2928$, $F = 19.89$

which highlight the importance of the electronic and steric properties of the phenyl substituents in modulating retention on the investigated CSP.

As shown by the correlation matrix (Table 2), log *k*' values of the two enantiomers are correlated for the set of compounds **3–16**, but a closer inspection of the scatter plot (Fig. S4, Supporting Information) pointed out two groups of points mostly lying on two almost parallel lines. The separate regression analysis yielded two linear equations ($r^2 > 0.81$) with similar slope (ca. 0.9) and different intercept, one gathering the majority of the *meta*-substituted compounds and the other gathering the majority of the *para*-substituted compounds, with intercepts of +0.25 and +0.12, respectively. This trend supports the fact that the second-eluted enantiomer of the *meta*-substituted compound is more retained compared to that of the *para*-substituted compound. Some deviations from the two almost parallel linear equations seem related to the bulkiness of substituents (limited steric fit). The incorporation in the regression equation of V_W and an indicator variable, which assumes the value of 1 for *meta*-substituents and 0 for *para*-substituents, led to the following equations:

$$\log k'_2 = 0.94\ (\pm 0.14) \log k'_1 - 0.08\ (\pm 0.03)\ V_W + 0.26\ (\pm 0.05) \quad (4)$$

$n = 14$, $r^2 = 0.8042$, $q^2 = 0.6534$, $s = 0.0908$, $F = 22.59$

$$\log k'_2 = 1.01\ (\pm 0.11) \log k'_1 - 0.09\ (\pm 0.02)\ V_W + 0.11\ (\pm 0.04)\ I_m + 0.21\ (\pm 0.05) \quad (5)$$

$n = 14$, $r^2 = 0.8905$, $q^2 = 0.7640$, $s = 0.0712$, $F = 27.10$

Eq. 5, which explains about 90% of the variance in the data, highlights the key roles of the steric properties of the aromatic substituents and substitution pattern (*meta* better than *para*) in driving the enantioselective retention of the piperidin-3-yl coumarin selectands on the amylose-based CSP. As a confirmation, log α, with the only exception of the 4-OMe derivative (**15**), reasonably correlates mainly with V_W (negative effect) and I_m (positive effect):

$$\log \alpha = -0.09\ (\pm\ 0.02)\ V_W + 0.13\ (\pm\ 0.03)\ I_m + 0.20\ (\pm\ 0.03) \quad (6)$$

$n = 13$, $r^2 = 0.7547$, $q^2 = 0.5430$, $s = 0.0589$, $F = 15.38$

Molecular modeling studies can usefully complement the above LFER equations, contributing to a better understanding of the intermolecular forces governing the enantioselective binding of the piperidin-3-yl coumarin derivatives to ADMPC CS. The 3D model of ADMPC CS (12-mer) was built as reported in Section 2.

The 3D structure of the ADMPC CS (12-mer) shows on its molecular surface differently accessible and shaped crevices or clefts, where enantiomers of racemic small molecules could selectively bind (Fig. 3). The highest-scored binding poses of a number of piperidin-3-yl coumarin derivatives (**2**, **3**, **6**, **7** and **8**) to ADMPC (12-mer) CS, as identified by molecular docking calculations, are shown in Fig. 4, and in Figs. S5 and S6 (Supporting Information). Docking calculations showed that the highest number of interactions stabilizing the SA-CS transient complexes were achieved by *S* enantiomers and that no significant difference exist in the binding modes of the selectands in neutral and protonated forms.

In general, the common 3,4-dimethylcoumarin moiety is involved in strong face-to-face and face-to-edge π–π interactions with the 3,5-dimethylphenyl of the ADMPC CS. The OH group of the 1-hydroxypropyl chain anchors compound **2** to an inner cleft of CS interacting with a carbamoyl NH by HB, whereas the benzyl group in **3** achieves π-stacking interactions with two 3,5-dimethylphenyl moieties of the ADMPC (Fig S5).

The *S* enantiomers of **6**, **7** and **8** also achieve binding poses similar to that of **3** (Fig. 4). In addition, fluorine (**6**) and CH_2OH (**7**) in *meta* position may interact with a carbamoyl NH through HB formation, whereas the 3-NO_2 group of **8** accepts HBs from carbamoyl NHs.

As for *rac*-**8**, distinctly different binding poses were identified as the best and most populated ones by molecular docking calculations of *S* and *R* enantiomers (Fig. S6). As for the *S* enantiomer, the 3-NO_2-phenyl moiety is deeply merged within ADMPC CS, achieving strong π–π interactions with 3,5-dimethylphenyl groups, strengthen by HBs involving the NO_2 group as acceptor. In contrast, the *R* enantiomer exposes the 3-NO_2-phenyl ring toward the solvent. The difference in free energies of binding of the *S* and *R* enantiomer (–15.84 and –14.83 kcal/mol, respectively), further supports the observed enantioselectivity.

4 Concluding remarks

The enantiomer resolution of a series of bioactive racemic 7-[(1-alkylpiperidin-3-yl)methoxy]coumarin derivatives was successfully achieved through enantioselective HPLC on an amylose-based CSP (Chiralpak IA; amylose tris(3,5-dimethylphenylcarbamate) as chiral selector), used in polar mode (MeOH/ACN, 8:2 v/v). The majority of the investigated selectands, especially those bearing 1-(3-X-benzyl)piperidin-3-yl moieties, showed baseline enantiomer separations, *rac*-**8** (X = NO_2) being the best resolved one ($\alpha = 2.01$; $R_S = 4.27$). The chromatographic data of this study support the scalability of the optimized experimental conditions (CSP and mobile phase) from analytical to preparative scale, allowing sufficient amount of each enantiomer for biological testing to be rapidly produced.

A number of LFER equations were also derived for the racemic compounds **3–16**, which highlighted a major role of electronic features, as accounted for by Hammett sigma constant of the X substituent, in modulating retention on the amylose-based CSP. The Hammett constant, in this SA series, should mainly describe the effect of the aromatic substituent on the propensity of the terminal phenyl group in the SA to graft π–π interaction with π-rich ADMPC moieties in CS. Molecular docking calculations confirmed the importance, in

modulating the enantioselective retention, of face-to-face and face-to-edge aromatic interactions between π-donor moieties in CS and π-acceptor moieties in SA, strengthened by HB interaction between HB donor (i.e., carbamoyl NH) in CS and HB acceptor group(s) in SA. The most statistically reliable LFER eq. 5 highlighted the key roles of the substituent's size and substitution pattern (*meta* better than *para*) in driving the enantioselective retention of the piperidin-3-yl-bearing coumarin selectands on the ADMPC CSP (Chiralpak IA).

Acknowledgements

L.P. acknowledges financial support from APQ Research Apulian Region "FutureInResearch (FKY7YJ5)—Regional program for smart specialization and social and environmental sustainability" - Fondo di Sviluppo e Coesione 2007–2013.

The authors have declared no conflict of interest

5 References

[1] Aboud-Enein, H.Y., Wainer, L.W. (Eds.) The impact of stereochemistry on drug development and use, Wiley, New York, 1997.

[2] Leek, H., Andersson, S. Preparative scale resolution of enantiomers enables accelerated drug discovery and development. *Molecules* 2017, *22*, 158.

[3] Leek, H., Thunberg, L., Jonson, A.C., Öhlén, K., Klarqvist, M. Strategy for large-scale isolation of enantiomers in drug discovery. *Drug Discov. Today* 2017, *22*, 133-139.

[4] Franco, P., Senso, A., Oliveros, L., Minguillón, C. Covalently bonded polysaccharide derivatives as chiral stationary phases in high-performance liquid chromatography. *J. Chromatogr. A*. 2001, *906*, 155-170.

[5] Chen, X. M., Yamamoto, C., Okamoto, Y. Polysaccharide derivatives as useful chiral stationary phases in high-performance liquid chromatography. *Pure Appl. Chem.* 2007, *79*, 1561-1573.

[6] Okamoto, Y., Ikai, T. Chiral HPLC for efficient resolution of enantiomers. *Chem. Soc. Rev.* 2008, *37*, 2593-2608.

[7] Kasat, R. B., Wang, N.-H. L., Franses, E.I. Effects of backbone and side chain on the molecular environments of chiral cavities in polysaccharide-based biopolymers. *Biomacromolecules* 2007, *8*, 1676-1685.

[8] Yamamoto, C., Yashima, E., Okamoto, Y. Structural analysis of amylose tris(3,5-dimethylphenylcarbamate) by NMR relevant to its chiral recognition mechanism in HPLC. *J. Am. Chem. Soc.* 2002, *124*, 12583-12589.

[9] Lämmerhofer, M. Chiral recognition by enantioselective liquid chromatography: mechanisms and modern chiral stationary phases. *J. Chromatogr. A* 2010, *1217*, 814-856.

[10] Pisani, L., De Palma, A., Giangregorio, N., Miniero, D. V., Pesce, P., Nicolotti, O., Campagna, F., Altomare C. D., Catto M. Mannich base approach to 5-methoxyisatin 3-(4-isopropylphenyl)hydrazone: A water-soluble prodrug for a multitarget inhibition of cholinesterases, beta-amyloid fibrillization and oligomer-induced cytotoxicity. *Eur. J. Pharm. Sci.* 2017, *109*, 381-388.

[11] Pisani, L., Catto, M., De Palma, A., Farina, R., Cellamare, S., Altomare, C. D. Discovery of potent dual binding site acetylcholinesterase inhibitors via homo- and heterodimerization of coumarin-based moieties. *ChemMedChem* 2017, *12*, 1349-1358.

[12] Farina, R.; Pisani, L.; Catto, M.; Nicolotti, O.; Gadaleta, D.; Denora, N.; Soto-Otero, R.; Mendez-Alvarez, E.; Passos, C. S.; Muncipinto, G.; Altomare, C. D.; Nurisso, A.; Carrupt, P. A.; Carotti, A. Structure-based design and optimization of multitarget-directed 2*H*-chromen-

2-one derivatives as potent inhibitors of monoamine oxidase B and cholinesterases. *J. Med. Chem.* 2015, *58*, 5561−5578.

[13] de Candia, M., Zaetta, G., Denora, N., Tricarico, D., Majellaro, M., Cellamare, S., Altomare, C. D. New azepino[4,3-b]indole derivatives as nanomolar selective inhibitors of human butyrylcholinesterase showing protective effects against NMDA-induced neurotoxicity. *Eur. J. Med. Chem.* 2017, *125*, 288-298.

[14] Pisani, L., Farina, R., Catto, M., Iacobazzi, R., Nicolotti, O., Cellamare, S., Mangiatordi, G., Denora, N., Soto-Otero, R., Siragusa, L., Altomare, C., Carotti, A. Exploring basic tail modifications of coumarin-based dual acetylcholinesterase-monoamine oxidase B inhibitors: Identification of water-soluble, brain-permeant neuroprotective multitarget agents. *J. Med. Chem.* 2016, *59*, 6791-6806.

[15] Soto-Otero, R., Mendez-Alvarez, E., Sanchez-Iglesias, S., Zubkov, F. I., Voskressensky, L. G., Varlamov, A. V., de Candia, M., Altomare, C. D. Inhibition of 6-hydroxydopamine-induced oxidative damage by 4,5-dihydro-3*H*-2-benzazepine *N*-oxides. *Biochem. Pharmacol.* 2008, *75*, 1526-1537.

[16] Soto-Otero, R., Méndez-Álvarez, E., Sánchez-Iglesias, S., Labandeira-García, J. L., Rodríguez-Pallares, J., Zubkov, F. I., Zaytsev, V. P., Voskressensky, L. G., Varlamov, A. V., de Candia, M., F. Fiorella, F., Altomare, C. 2-Benzazepine nitrones protect dopaminergic neurons against 6-hydroxydopamine-induced oxidative toxicity. *Arch. Pharm.* 2012, *345*, 598-609.

[17] Schrödinger Release 2016-3: Maestro, Schrödinger, LLC, New York, NY, 2016.

[18] QUACPAC 1.7.0.2: OpenEye Scientific Software, Santa Fe, NM. http://www.eyesopen.com.

[19] http://polysac3db.cermav.cnrs.fr/home.html

[20] Imberty, A., Chanzy, H., Pérez, S., Buléon, A., Tran, V. The double-helical nature of the crystalline part of A-starch. *J. Mol. Biol.* 1988, *201*, 365-378.

[21] Schrödinger Release 2016-3: Desmond Molecular Dynamics System, D. E. Shaw Research, New York, NY, 2016. Maestro-Desmond Interoperability Tools, Schrödinger, New York, NY, 2016.

[22] Bowers, K. J., Chow, E., Xu, H., Dror, R. O., Eastwood, M. P., Gregersen, B. A., Klepeis, J. L., Kolossvary, I., Moraes, M. A., Sacerdoti, F. D., Salmon, J. K., Shan, Y., Shaw, D.E. Scalable algorithms for molecular dynamics simulations on commodity clusters, Proceedings of the ACM/IEEE Conference on Supercomputing (SC06), Tampa, Florida, 2006, November 11-17 (https://dl.acm.org/citation.cfm?id=1188455).

[23] Morris, G. M., Huey, R., Lindstrom, W., Sanner, M. F., Belew, R. K., Goodsell, D. S., Olson, A. J. AutoDock4 and AutoDockTools4: Automated docking with selective receptor flexibility. *J. Comput. Chem.* 2009, *30*, 2785-2791.

[24] Huey, R., Morris, G. M., Olson, A. J., Goodsell, D. S. A semiempirical free energy force field with charge-based desolvation. *J. Comput. Chem.* 2007, *28*, 1145-1152.

[25] Hawkins, P. C. D., Skillman, A. G., Nicholls, A. Comparison of shape-matching and docking as virtual screening tools. *J. Med. Chem.* 2007, *50*, 74-82.

[26] Hawkins, P. C., Skillman, A. G., Warren, G. L., Ellingson, B.A., Stahl, M. T. Conformer generation with OMEGA: algorithm and validation using high quality structures from the Protein Databank and Cambridge Structural Database. *J. Chem. Inf. Model.* 2010, 50, 572-584.

[27] Bezençon, J, Wittwer, M.B., Cutting, B., Smieško, M., Wagner, B., Kansy, M., Ernst, B. pK_a determination by ^1H NMR spectroscopy - an old methodology revisited. *J. Pharm. Biomed. Anal.* 2014, *93*, 147-155.

[28] Avdeef, A., Box, K. J., Comer, J. E. A., Gilges, M., Hadley, M., Hibbert, C., Patterson, W., Tam, K.Y. pH-metric log P 11. pKa determination of water-insoluble drugs in organic solvent-water mixtures. *J. Pharm. Biomed. Anal.* 1999, *20*, 631–641.

[29] Altomare, C., Carotti, A., Cellamare, S. Fanelli, F., Gasparrini, F., Villani, C., Carrupt, P.-A., Testa, B. Enantiomeric resolution of sulfoxides on a R, R-DACH- DNB chiral stationary phase: A quantitative structure-enantioselective retention relationship (QSERR) study. *Chirality* 1993, *5*, 527-537.

[30] Carotti, A., Altomare, C., Cellamare, S., Monforte, A. M., Bettoni, G., Loiodice, F., Tangari, N., Tortorella, V. LFER and CoMFA studies on optical resolution of alpha-alkyl alpha-aryloxy acetic acid methyl esters on DACH-DNB chiral stationary phase. *J. Comput. Aided Mol. Des.* 1995, *9*, 131-138.

[31] Altomare, C., Cellamare, S., Carotti, A., Barreca, M. L., Chimirri, A., Monforte, A. M., Gasparrini, F., Villani, C., Cirilli, M., Mazza, F. Substituent effects on the enantioselective retention of anti-HIV 5-aryl-delta 2-1,2,4-oxadiazolines on *R*,*R*-DACH-DNB chiral stationary phase. *Chirality* 1996, *8*, 556-566.

[32] Hansch, C., Leo, A. Substituent constants for correlation analysis in chemistry and biology, Wiley, New York, NY, 1979.

[33] van de Waterbeemd, H., Testa, B. The parametrization of lipophilicity and other structural and other structural properties in drug design in Advances in Drug Research (vol. 16). Academic Press London 1987, pp. 85-225.

[34] http://statist.wald.intevation.org/

Figure legends

Figure 1. Selector structures of the commercially available amylose-based CSPs used. Tradenames: A) Lux® Amylose-2; B) Chiralpak® IA.

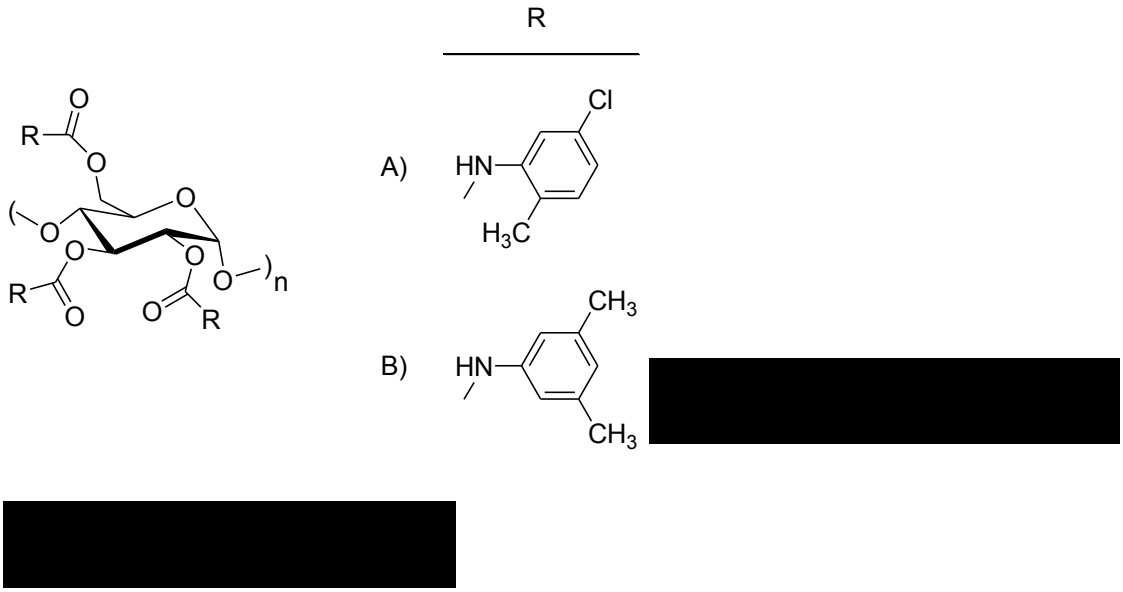

Figure 2. Chromatograms of **3**, **7** and **8** on Chiralpak® IA as the CSP and MeOH/ACN, 8:2 v/v, as the mobile phase; flow rate: 1 mL/min.

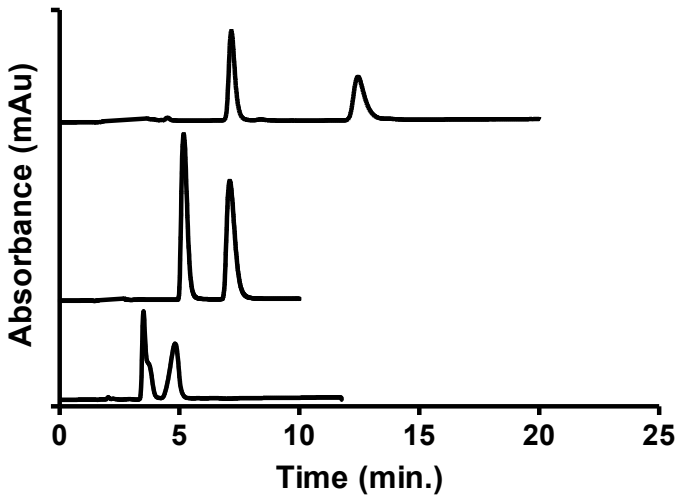

Figure 3. Two perspective views of the molecular surface of the 3D model of ADMPC (12-mer) chiral selector (Chiralpak IA), colored by atom type: C (green), O (red), N (blue), H (white).

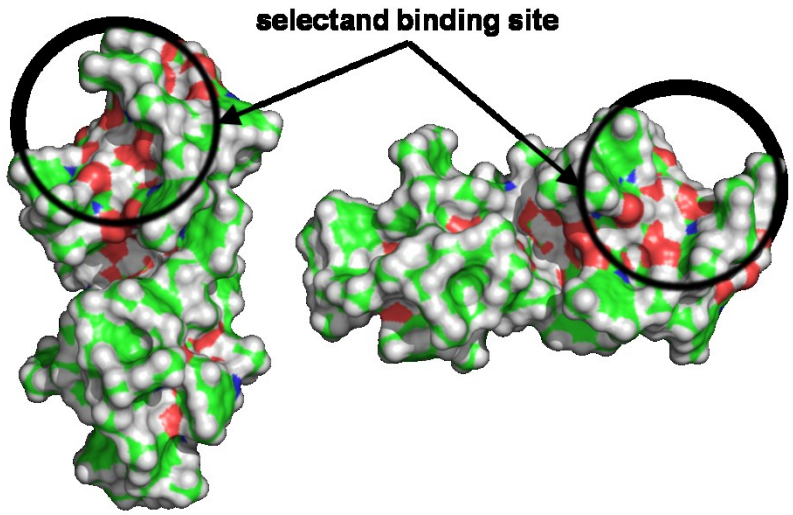

Figure 4. Best-scored binding poses of *S* enantiomers of **6** (right), **7** (center) and **8** (left) to the 3D structure of ADMPC (12-mer) CS, as assessed by molecular docking calculations. The estimated free energies of binding, according to the AutoDock scoring function, are -13.96, -14.73, and -16.25 kcal/mol, respectively. The interacting moieties of SA and CS are colored by atom type: C (yellow and green in SA and CS, respectively), O (red), N (blue), H (white); HB interactions in cyan-colored dashed lines.

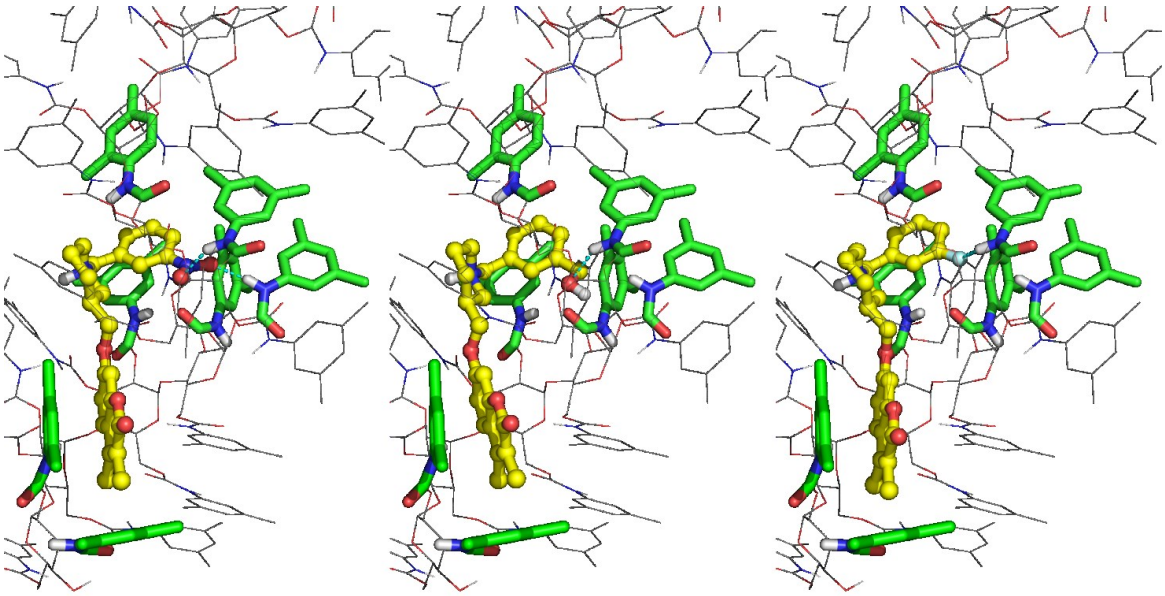

Table 1. HPLC enantiomer resolution data on Chiralpak IA CSP (mobile phase: MeOH/MeCN, 80:20 v/v) and lipophilicity parameters of *rac*-7-((1-alkylpiperidin-3-yl)methoxy)coumarin derivatives **1-16**.

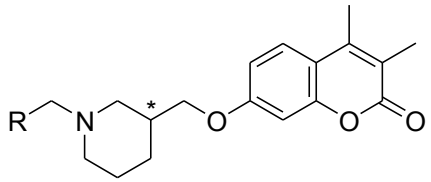

Cmpd	R	Enantiomer separation				Lipophilicity	
		k'_1	k'_2	α	R_S	log k'_w [a]	CLOGD [b]
1	H	1.80	-	1	-	1.34	0.58
2	CH_2CH_2OH	0.60	2.30	3.83	1.97	1.42	0.33
3	Ph	1.50 [c]	2.74 [c]	1.83	2.50	1.77	2.03
4	3-BrPh	2.29 [c]	3.48 [c]	1.52	1.88	2.16	2.81
5	3-ClPh	2.25	3.44	1.53	2.18	3.38	2.64
6	3-FPh	1.50	2.74	1.82	2.50	1.77	2.10
7	$3\text{-}CH_2OHPh$	0.76	1.42	1.86	1.19	1.65	0.85
8	$3\text{-}NO_2Ph$	2.69	5.42	2.01	4.27	1.42	1.82
9	4-ClPh	1.83	2.65	1.44	2.12	2.32	2.64
10	4-FPh	1.25	1.93	1.55	1.90	1.98	2.08
11	$4\text{-}CH_2OHPh$	1.09	-	1	-	1.53	0.85
12	$4\text{-}NO_2Ph$	3.77	4.20	1.11	0.72	1.57	1.87
13	$4\text{-}SO_2MePh$	3.09	-	1	-	0.47	0.39
14	4-CNPh	2.00	2.30	1.15	0.90	0.92	1.50

15	4-OCH_3Ph	2.37	3.73	1.57	2.25	2.25	1.94
16	3,4-$(OCH_3)_2$Ph	1.80	-	1	-	1.91	1.78

[a] RP-HPLC capacity factor extrapolated at 100% water volume fraction in aqueous mobile phase. [b] *n*-Octanol/water distribution coefficient at pH 4.00 as calculated with ACDLabs software, release 9.0 (Advanced Chemistry Development, Inc., Toronto, Canada). [c] The enantiomers were isolated by semi-preparative column [14]; $[\alpha]^{20}_{D}$ = -18.5° (*c* 0.13, MeOH) and -33.5° (*c* 0.08, MeOH) for the first eluted enantiomers of **3** and **4**, respectively.

Table 2. Correlation matrix (*r*) of the enantiomer separation data and the substituent physicochemical constants for the *meta*- and *para*-X-substituents used in multiple linear regression analysis of *rac*-7-((1-X-benzylpiperidin-3-yl)methoxy)coumarin derivatives (**3**-**16**, n = 14).[a]

	log *k*'$_1$	**log *k*'$_2$**	**log *α***	***σ***	***MR***	V_W	***τ***	π_{ar}
log *k*'$_1$	1							
log *k*'$_2$	0.839	1						
log *α*	-0,243	0.323	1					
σ	0.629	0.565	-0.084	1				
MR	0.347	0.018	-0.575	0.133	1			
V_W	0.254	-0.092	-0.609	0.038	0.979	1		
τ	-0.098	0.115	0.376	-0.403	-0.322	-0.335	1	
π_{ar}	0.185	0.413	0.417	-0.090	-0.433	-0.478	0.774	1

[a] σ, Hammett substituent constant; *MR*, molar refractivity; V_W, van der Waals volume; τ, lipophilic substituent parameter calculated from RP-HPLC log k'_w values as: log k'_w (RX) - log k'_w (RH); π_{ar}, Hansch lipophilic constant for the substituents on aromatic ring.